ADAPTIVE KUAN REGRESSIVE GENE OPTIMIZED FEATURE SELECTION BASED TUCKER'S CONGRUENCE DEEP CONVOLUTIONAL LEARNING FOR CHANGE DETECTION USING SATELLITE IMAGES

A. Jensila Smile and C. Immaculate Mary

Department of Computer Science, Sri Sarada College for Women, India

Abstract

Change detection in multi-temporal images is a remote sensing application detects land cover changes that occurred between two satellite images acquired at different times in same geographical region but different obtained from different types of sensors. Several research works have been conducted in change detection but accurate detection with minimum time still remains a challenging issue. A novel technique called Adaptive Kuan Regressive gene optimized feature selection-based Tucker's Congruence Deep Convolutional learning (AKRGOFS-TCDCL) is proposed for accurate change detection with minimum time. The proposed AKRGOFS-TCDCL technique involves three processes namely preprocessing, feature selection, and classification. Preprocessing of atmospheric corrections, radiometric correction, topographic correction, and contrast enhancement are performed using Adaptive Kuan filtering. With the preprocessed image, optimal features are selected by means of machine learning-based GA called Dichtomous probit Regression, for minimizing time consumption. Finally, classification is performed using Tucker's congruence coefficient deep convolutional neural learning for detecting changes in given satellite images via feature matching. In this way, accurate change detection is performed with minimum error. An experimental evaluation of the proposed AKRGOFS-TCDCL technique and existing methods are performed using satellite image dataset. The results are discussed with different performance metrics such as detection rate, false-positive rate, and detection time with respect to different satellite images.

Keywords:

Detection, Adaptive, Dichotomous, Tucker's Congruence

1. INTRODUCTION

Change detection capturing identical geographic bi-temporal satellite images acquired at different locations and time instances has great practical application with the swift development of satellite technology. To be more specific, change detection is said to be a fundamental task in computer vision involving diversified applications like, intelligent security, national defense, fire detection, and intelligent transportation, and so on.

A deep Siamese Convolutional Multiple-Layers Recurrent Neural Network (SiamCRNN) was developed in [1] for identifying the changes using multitemporal images. The developed SiamCRNN was not efficient to perform accurate detection with minimum time consumption. An attention mechanism-based deep supervision network (ADS-Net) was developed in [2] for change detection using bi-temporal remote sensing images. The designed network structure failed to precisely detect various changes.

A shape-aware siamese convolutional network (SASCNet) was developed in [3] to concurrently incorporate different information for identifying changes. But the accuracy of change detection was not improved. A new hierarchical Bayesian model was introduced in [4] for identifying various changes. However, time consumption of change detection was not analyzed. A novel technique based on superpixel segmentation and image regression was introduced in [5] to identify changes among bitemporal synthetic aperture radar images. However, the designed framework performing reconstruction for each pixel involved high complexity.

A new self-supervised representation learning technique was introduced in [6] for predicting changes detection for remote sensing images. However, it failed to consider other homogeneous images for change detection. A patch level and pixel-level change detection were performed in [7] for bitemporal remote sensing images with the extracted features to improve change detection effectiveness. But it failed to perform accurate change detection with multiple high-resolution remote sensing images.

An unsupervised change detection scheme was introduced in [8] for increasing accuracy and minimizing error. However, change detection time consumption was not minimized. A Fast Spatiotemporal Tree Filter (FSTF) was introduced in [9] to boost binary detection using different types of change detection methods. But it failed in considering simultaneously multiple object masks with same image. A new hybrid machine learning technique was introduced in [10] for change detection from satellite images. The designed technique increased change detection accuracy but it failed to validate the performance with respect to time consumption.

In satellite images, change detection (CD) technology has become more important for determining differences in the object or event at dissimilar times. Numerous conventional research works were developed to detect the changes. But, the accuracy of detection using traditional methods is not sufficiently improved. Therefore, few research works have been implemented to perform pre-processing of images. However, the amount of time needed for efficient change detection. Thus, it failed to increase the detection performance of satellite images. Motivated by, a novel AKRGOFS-TCDCL technique is proposed.

The major contributions of this work are illustrated as given below,

AKRGOFS-TCDCL technique is introduced to accurately identify the change detection with lesser time. Proposed technique involving distinct processes namely preprocessing, feature selection, feature extraction, and classification. At first, AKRGOFS-TCDCL is to perform preprocessing of image with atmospheric corrections, radiometric correction, topographic correction, and contrast enhancement by means of Adaptive Kuan filter. This is helps to remove the noise and enhance the image quality. Secondly, proposed technique utilizes Dichotomous probit Regressive gene optimization is to identify the optimal

feature based on texture, color, and intensity. Finally, Tucker's congruence coefficient deep convolutional neural learning is applied for detection various changes with satellite images via feature matching.

The main objective of the research work described as follows.

- To enhance change detection with remote sensing images, novel deep learning-based technique called AKRGOFS-TCDCL is proposed.
- To improve image quality, Adaptive Kuan filter is used in the AKRGOFS-TCDCL technique.
- To reduce the change detection time, Dichotomous probit Regressive gene optimized feature selection is applied in the proposed technique.
- To find the various changes in satellite images, Tucker's congruence coefficient deep convolutional neural learning is introduced in the AKRGOFS-TCDCL technique.

The rest of this paper is arranged into five different sections. Section 2 discusses the related works. Section 3 describes the proposed AKRGOFS-TCDCL with a neat diagram. In section 3, simulation settings are presented with different parameters. The performance analyses with various performance metrics are discussed in section 4. The conclusion of this paper is presented in section 5.

2. RELATED WORKS

An α-cut induced Fuzzy layer to Deep Neural Network (αFDNN) was introduced in [11] to improve change detection accuracy. But preprocessing concerning various corrections was not performed to further improve the accuracy. Convolutional Neural Network was introduced in [12] for change detection based on designed loss function for optical aerial images. However, it failed to directly use multitemporal images to learn multiple features.

An advanced superpixel-based Markov random field (MRF) method was developed in [13] for change detection. The designed method was not found to be efficient in removing false-alarm superpixels. A bilinear convolutional neural network (BCNNs) was developed in [14] to identify changes in bitemporal multispectral images based on deep features learning. The designed BCNNs were not efficient in concentrating on the accuracy aspect.

Edge-preserving memory-based cumulative sum (MB-CUSUM) methods were introduced in [15] for detecting abrupt changes. The designed methods achieved superior performance but change detection complexity was not focused. A feature-level U-Net algorithm was introduced in [16] for identifying changes from multi-spectral images. However, the designed algorithm was not found to be efficient involving complex scenes.

An integrated filtering method was introduced in [17] to improve change detection. But the performance of detection enhancement was not improved. A Bipartite Differential Neural Network (BDNN) was introduced in [18] for unsupervised image change detection. However, the time complexity involved in image change detection was not focused.

A novel SAR image enhancement technique was developed in [19] for change detection. The designed technique failed to improve change detection accuracy of the image. A hierarchical dynamic fusion network (HDFNet) was introduced in [20] for aerial image-change detection. But the designed network failed to consider multiscale features.

Motivated by the above said issues, in this work, technique called Adaptive Kuan Regressive gene optimized feature selection-based Tucker's Congruence Deep Convolutional learning (AKRGOFS-TCDCL) is designed for accurate change detection with minimum time.

3. METHODOLOGY

With improvement in satellite technology, different numbers of remote sensing images are captured from similar regions at different times. Numerous remote sensing images are acquired by various imaging sensors. Change detection is a significant process of finding the variations of an object or events from the remote sensing images. On the basis of the captured images, comparative analysis between modified regions and non-modified regions are made. In our work, three different processes like, preprocessing feature selection and classification are applied to the input satellite images with the objective of detecting accurate changes. The Fig.1 given below shows the architecture of AKRGOFS-TCDCL technique.
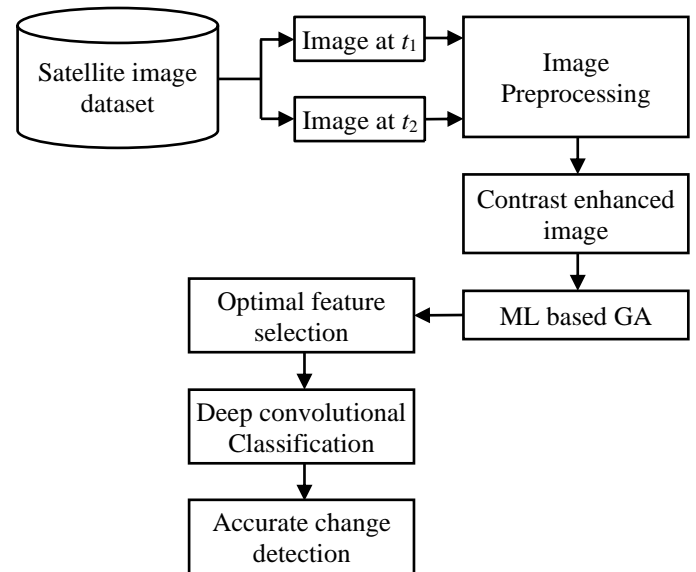

Fig.1. Architecture of AKRGOFS-TCDCL Technique

As shown in the above figure, to start with, different numbers of satellite land images L_1, L_2, L_3,…,L_n acquired at different times are provided as input to monitor the change. Followed by which image preprocessing is carried out to perform different corrections and noise removal to obtain quality enhanced input image. Next, machine learning-based genetic algorithm is applied to select and extract optimal feature. Finally, to the extracted optimal features classification is performed using Deep Convolutional neural learning. This is helps to improve the accurate change detection. The detailed processes of AKRGOFS-TCDCL technique are described in the following section.

3.1 PREPROCESSING

Satellite images obtained from Landsat sensors are found to be highly distorted due to great influences from atmospheric and topographic conditions, therefore compromising the change detection. Preprocessing in our work is performed to reduce these ill effects. However, preprocessing performed for change detection in the literature are found to be time-consuming and also at certain cases incorrectly removes the artifacts. To address this issue, in our work preprocessing is performed by concentrating on the atmospheric correction, radiometric correction, topographic correction, and contrast enhancement.

First, atmospheric correction is done using Dark Object Subtraction to eliminate the effects of atmosphere on reflectance values of land images acquired from satellite. The atmospheric correction in our work using Dark Object Subtraction is given below,

$$r_\lambda = \frac{\pi * v^2 * \left(R_{\lambda_s} - R_{\lambda_p}\right)}{\left(R_{\lambda_{ex}} * \cos(\theta_Z)\right)} \qquad (1)$$

$$R_{\lambda_s} = d_{n_{cl}} * G_\lambda + B_\lambda \qquad (2)$$

From the above Eq.(1) and Eq.(2), the surface reflectance 'r_λ' value is obtained based on the product of a constant '$\pi = 3.14$' and distance between earth and sun 'v', difference between spectral radiance at the sensor's aperture '$R_{\lambda s}$' and path radiance '$R_{\lambda p}$' with respect to the product of Exo-atmospheric solar spectral irradiance '$R_{\lambda ex}$' and the solar zenith angle '$\cos\theta_z$' respectively. Followed by which the spectral radiance at the sensor's aperture '$R_{\lambda s}$' is estimated based on the quantized calibrated pixel value of each sensor image 'dn_{cl}', radiometric gain 'G_λ' and radiometric bias 'B_λ' respectively.

Followed by atmospheric correction, radiometric correction is performed as a preprocessing step in our work to eliminate radiometric errors and remove geometric distortion. To be more specific, radiometric correction is performed to remove radiometric variation between multi temporal high-resolution images caused by various sun angles, light intensity, and atmospheric conditions. In our work, radiometric correction is performed by means of radiometric relative normalization. The radiometric relative normalization varies the range of pixel intensity values between 0 and 255 using min-max normalization. This is mathematically expressed is given below,

$$N(p_i) = \frac{p_i - p_{mn}}{p_{mx} - p_{mn}} \qquad (3)$$

From Eq.(4), the min-max normalization of the satellite image pixels 'N_{pi}', are obtained on the basis of the original pixel value 'p_i', minimum pixel value 'p_{mn}', and the maximum pixel value 'p_{mx}'. The third correction performed in the preprocessing stage is the topographic correction that assists in eliminating the ill effects of topography. This topographic correction is performed in our work by means of Lambertian function as given below.

$$T_h = \rho_t * \left[\frac{\cos\theta_s}{\cos\alpha}\right] \qquad (4)$$

From Eq.(4), the topographic correction for the corresponding horizontal surface 'T_h' is done based on the reflectance of an inclined terrain 'ρ_t' and the ratio of terrain slope '$\cos\theta_z$' with

respect to the solar illumination angle '$\cos\alpha$' respectively. Finally, the contrast-enhanced image for accurate change detection is obtained by means of Adaptive Kuan filtering technique that in turn removes the noise and enhances the satellite image quality, therefore contributing to overall detection rate. For an overall of $n*n$ filtering window, let us consider an input satellite image 'L_i' and number of pixels be represented by $p_1, p_2, p_3,\ldots p_n$. To start with, the image pixels are positioned in ascending order and center value in the filtering window is obtained.

p_1	p_2	p_3
p_4	p_{ij}	p_6
p_7	p_8	p_9

Fig.2. 3×3 Filtering Window

With even number of pixels in center nine different pixels are arranged with central coordinates of a pixel in the window represented as (p_{ij}) as given in Fig.2. Then, the filtered output is represented as given below,

$$Q = \mu + \|p_{ij} - \mu\| * \delta \qquad (5)$$

From the above Eq.(5), the filtered output 'Q' is obtained based on the local mean inside filtering window 'μ', difference between central pixel and local mean '$p_{ij}-\mu$' to the product of the weight 'δ' respectively. The pixel that deviates from mean value is filtered out from satellite images. With this, the contrast-enhanced image forms the resultant preprocessed image.

Algorithm 1: Satellite Image preprocessing

Input: Dataset, satellite images $L_1, L_2, L_3,\ldots, L_n$

Output: Preprocessed image

Begin
Step 1: For each satellite image $L_i(t_1)$ and is $L_i(t_2)$
Step 2: Perform Atmospheric corrections using Dark Object Subtraction method r_λ
Step 3: Apply min-max normalization for Radiometric correction $N(p_i)$
Step 4: Apply Lambertian method for topographic correction T_h
Step 5: Apply Adaptive Kuan filtering
Step 6: Extract the number of pixels $p_1, p_2, p_3,\ldots p_n$
Step 7: Arrange the pixels in filtering with ascending order
Step 8: Take center pixel value p_{ij}
Step 9: Find pixels that deviate from the center pixel value
Step 10: Remove the noisy pixels
Step 11: return (contrast-enhanced image)
Step 12: End for
End

The above algorithm provides step-by-step process of satellite image preprocessing to obtain quality enhanced image. For each input satellite image, first, atmospheric correction is done using Dark Object Subtraction method. Followed by which, with the atmospheric corrected image, second, the radiometric correction is carried out using the min-max normalization method. Third, to the radiometric corrected image, Lambertian method is applied for topographic correction. Finally, to the topographic corrected satellite image, Adaptive Kuan filtering technique is applied to remove noisy pixel that deviates from center pixel value. As a result, contrast-enhanced smooth image is obtained.

3.2 DICHOTOMOUS PROBIT REGRESSIVE GENE OPTIMIZED FEATURE SELECTION

With the preprocessed satellite images pertinent features for change detection has to be observed. In our work optimal feature selection and extraction are performed using Dichotomous probit Regressive gene optimization. The objective behind the design of Dichotomous probit Regressive gene optimization algorithm is to search the best feature in an adaptive manner and finally obtain the optimal features. On the contrary to conventional genetic algorithm, the Dichotomous probit regression used in our work improves the optimization performance by estimating the relationships between a variable i.e. 'features'. With the features of the satellite images being texture (t), intensity (I), and color (c), the combinations are formed in an arbitrary fashion to model initial population as given below.

$$W_i = C_1, C, C_3, \ldots . C_m \qquad (6)$$

From Eq.(6), W_i denotes a feature combination $C_1, C, C_3, \ldots . C_m$ i.e $C_1 = (t,I,c)$, $C_2 = (t,c)$, $C_3 = (t,I)$ and so on. Among the multiple feature combinations, optimal feature is chosen for classification with minimum time on the basis of the fitness function employing Dichotomous probit regression with the objective of reducing the error. The Dichotomous probit regression function analyzes the feature combination and selects the best optimal feature, by returning two outcomes and hence it is called Dichotomous regression.

$$R = \begin{cases} 1 & E < th \\ 0 & E \geq th \end{cases} \qquad (7)$$

From the Eq.(7), the regression outcomes 'R' are obtained based on the conditionality checking between the threshold 'th' and error factor 'E'. If the error value is found to be less than the threshold the regression outcomes returns '1'. Otherwise, the regression outcome returns '0'. Based on the fitness computation, the optimal fittest feature combination is chosen for classification. Followed by regression outcomes, truncation selection, ring crossovers, and Gaussian mutation are performed to obtain optimal feature combination.

The proposed technique uses truncation selection for selecting the best chromosomes based on their current fitness value. Initially, feature combinations are sorted based on their current fitness. After sorting the feature combinations, then the truncation process is applied to select the best individuals. Only the individual's error value below the threshold is selected for the next recombination process (i.e. crossover). The Individual's error value higher than the threshold does not produce offspring during the recombination. Hence, the individual's error wit higher value is removed. In this way, the best individuals are selected from the population for the recombination process.

The next process is the crossover that handles more than one parent solutions generating offspring's (i.e. children's) via swapping process. The ring crossover operator is used for optimal selection. The binary representation of the chromosomes are $A = b_1, b_2, b_3, \ldots, b_n$ and $B = s_1, s_2, s_3 \ldots . s_n$. Then the offspring is generated as shown in Fig.4.
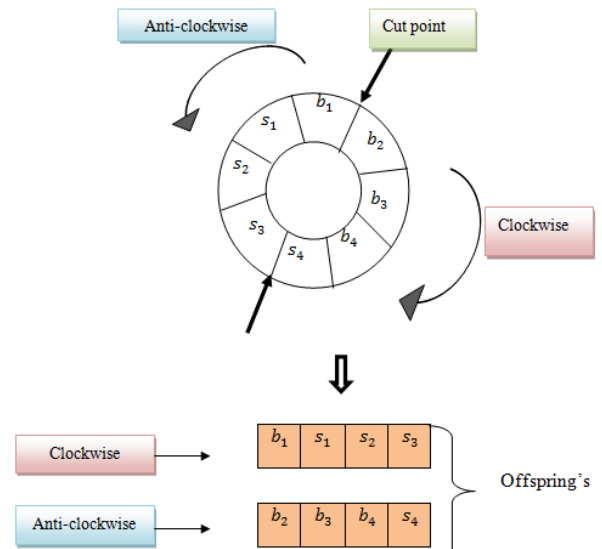

Fig.3. Ring crossover

The Fig.3 shows the process of ring crossover to generate offspring from parent solutions. The crossover is performed on the basis of the combination of two-parent solutions with the purpose of providing new adapted ones. The obtained offspring string length is similar to total string length of both parents and owing to the application of ring crossover, the process does not make diversity within a population. Hence, to maintain diversity bio-inspired operator called mutation is applied in our work.

After offspring's generation, mutation process is carried out to generate new offspring. In our work, Gaussian Mutation is employed to randomly alter chromosome bits. It also assists in preserving the genetic diversity from one generation to next generation. The Gaussian mutation function is expressed as given below,

$$G = \frac{1}{\sqrt{2\pi d^2}} * \exp\left(-\frac{r^2}{2d^2}\right) \qquad (8)$$

From the Eq.(8), the newly generated offspring 'G' is obtained based on the variance 'd', Gaussian normally distributed random number with 0 mean and variance 1 represented by 'r'. Based on the Gaussian mutation operator, the bits are interchanged as given below,
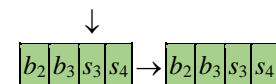

Fig.4. Gaussian Bit String Mutation

The Fig.4 illustrates the Gaussian bit string mutation that generates new offspring to select optimal feature combination. As a result, a novel offspring is generated that in turn calculates the fitness to identify the fittest combination features. This process is said to be repeated until obtaining maximum iteration. After the best combination selection, various features are selected, i.e., texture feature, intensity feature and color feature respectively.

The texture feature of the image offers spatial information of pixels intensities that are extracted as given below:

$$T_x = \frac{\sum_i \sum_j (p_i - m_i)(p_j - m_j)}{\sigma_i * \sigma_j} \qquad (9)$$

From the Eq.(9), the texture feature are obtained 'T_x' based on the mean of the pixels 'm_i and m_j' and their deviations 'σ_i and σ_j' respectively. Then, the intensity feature of the image is measured as the difference between actual pixels and their neighboring pixels as given below.

$$Int = \sum_i \sum_j \| p_i - p_j \|^2 \qquad (10)$$

From the Eq.(10), the intensity 'Int' feature of the image is obtained based on the actual pixels 'p_i' and their neighboring pixels 'p_j'. Finally, the color feature from the input satellite image is converted into the HSV (hue, saturation, value) as given below.

$$m_{hsv} = \frac{1}{n} * Int \qquad (11)$$

From the Eq.(11), the mean of the HSV 'm_{hsv}' is estimated based on the pixel intensity 'Int' and total number of pixels 'n' in image. Based on the mean value, the variance is estimated as given below,

$$\sigma_{hsv}^2 = \frac{1}{n} \sum (Int - m_{hsv})^2 \qquad (12)$$

From Eq.(12), the variance of HSV 'σ^2_{hsv}' is estimated based on the difference between the pixel intensity 'Int' and the mean of HSV 'm_{hsv}' respectively. Finally, the skewness is calculated as follows,

$$\varphi_f = \frac{\frac{1}{n} \sum (Int - m_{hsv})^3}{\left(\frac{1}{n} \sum (Int - m_{hsv})^2 \right)^{1.5}} \qquad (13)$$

From the Eq.(13), the skewness 'φ_f' is measured on the basis of mean of HSV 'm_{hsv}'. Based on the above-said mean, variance, and skewness, the color features are extracted. The algorithmic process of the Dichotomous probit Regressive gene optimized feature selection is given below,

Algorithm 2 Dichotomous probit Regressive gene optimized feature selection

Input: Preprocessed Image $L_1, L_2, L_3, \ldots, L_n$

Output: Select and extract the optimal features

Begin

Step 1: Initialize the population of feature combination $W_i = C_1, C_2, C_3, \ldots, C_m$

Step 2: for each $C_i \in W_i$

Step 3 Calculate the fitness based on regression

Step 4: if (maximum iteration is met) **then**

Step 5: Selects an optimal combination

Step 6: else

Step 7: Apply truncation selection

Step 8: if ($f > f_{th}$) then

Step 9: Select a parent chromosome

Step 10: else

Step 11: Select another chromosome

Step 12: end if

Step 13: Apply ring crossover to generate new offspring

Step 14: Perform Gaussian Mutation

Step 15: Replace old individual into a new one

Step 16: Go to step 4

Step 17: **End if**

Step 18: **End for**

Step 19: Extract the texture features T_x, intensity features *Int*, color features m_{hsv}, σ^2_{hsv}, φ_f

End

Algorithm 2 describes the pseudo code representation of Dichotomous probit Regressive gene optimized feature selection. To start with, the feature combination population is initialized in a random manner. After that, the fitness of each feature combination is computed based on the regression function. If the error rate is comparatively lesser than the threshold, the regression function returns '1', followed by which the feature combination is selected. On contrary, the regression function returns '0'. Next, on the basis of fitness, the truncation selection is performed to select the current best individual among the population. Then the ring crossover is modelled to obtain two offspring. Followed by, the Gaussian mutation is applied to invert the bit randomly and again computes the fitness criteria. This process is continued until the maximum iteration gets reached.

3.3 TUCKER'S CONGRUENCE COEFFICIENT DEEP CONVOLUTIONAL NEURAL LEARNING

Finally, based on the extracted optimal features classification is performed using Tucker's Congruence Coefficient Deep Convolutional neural learning to identify the changes in remote sensing images with higher accuracy. Deep learning technique uses numerous layers in the network to gradually examine higher-level features from raw input satellite images. Deep Convolutional neural learning includes multiple layers such as an input layer, hidden layers, and an output layer. In convolutional neural network, hidden layers include a layer that performs a convolution operation whereas the input feature vector contributes to input of the next layer. This is followed by other layers such as pooling layers, fully connected layers, and normalization layers.

Pooling layers are used to minimize feature input dimensions by integrating neuron outputs at one layer into a single neuron in the next layer. On the other hand, the fully connected layers link each neuron in one layer associated with the neuron in another layer. Finally, the normalization layer normalizes input features.
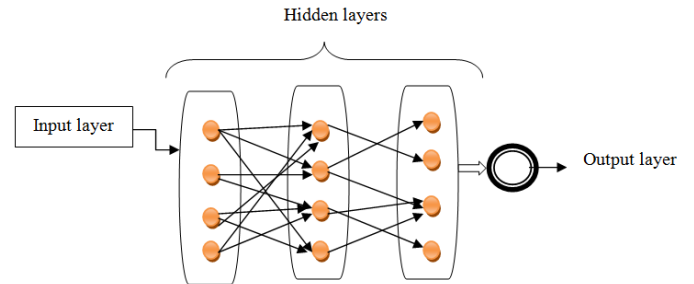

Fig.5. Architecture of Tucker's Congruence Coefficient Deep Convolutional Neural Learning

The Fig.5 depicts the architecture of Tucker's Congruence Coefficient Deep Convolutional neural learning with different layers. Deep Convolutional neural learning includes one input layer, hidden layers, and one output layer. In the input layer, the numbers of satellite land images are collected from the satellite image dataset. Each input image to the input layer is then sent to the nodes in hidden layer. The proposed AKRGOFS-TCDCL technique work also able to variance the number of satellite land images for feature processing till it is sent to the hidden layer. In hidden layers, the Tucker's Congruence Coefficient is used to examine the features. The extracted features are transferring one layer to another layer by using neurons in the network. In the output layer, the classification is used to discover the changes as correctly detected or not correctly detected.

Let us consider an input satellite image dataset comprises a huge number of satellite land images denoted as '$L_1, L_2, L_3,…,L_n$'. The extracted features are given as input to the input layer at time 't' with the adjustable weights. The activity of neuron at the input layer is expressed as given below,

$$x(t) = c + \sum_{i=1}^{q} w_i * F_i(t) \tag{14}$$

From Eq.(14), $x(t)$ indicates neuron activity at the input layer, w_i denotes a weight which is a random number that helps to make stronger connection between layers, $F_i(t)$ indicates an input feature vector, c denotes a bias that stores the value as '+1'. Then the inputs are transferred to the hidden layers. In that layer, Tucker's Congruence Coefficient is applied to measure correction between features extracted from two satellite images.

$$Z_{ij} = \frac{\sum F_i(t_i) * F_j(t_j)}{\sqrt{\sum F_i(t_i)^2 * \sum F_j(t_j)^2}} \tag{15}$$

From the Eq.(15), Tucker's congruence correlation coefficient 'Z_{ij}' is obtained on the basis of sum of the product of paired score of two features '$\sum F_i(t_i)*F_j(t_j)$' and the squared score of F_i'$\sum F_i(t_i)^2$', squared score of '$F_j\sum F_j(t_j)^2$'. The Tucker's congruence correlation coefficient (Z_{ij}) provides values ranging between '-1' and '+1'. The coefficient with '+1' indicates a positive correlation whereas '-1' represents a negative correlation between two features.

$$Z_{ij} = \begin{cases} +1 & \text{Changes not detected} \\ -1 & \text{Changes detected} \end{cases} \tag{16}$$

The value of '-1' indicates that the features of one image varies from the other image whereas the value of '+1' indicates that the features of one image does not varies from the other images. In this way, the changes are detected based on feature matching in the two homogeneous images.

Then the output of the hidden layer is expressed as follows,

$$H(t) = \sum_{i=1}^{q} w_1 * F_i(t) + \left[w_2 * h(t-1) \right] \tag{17}$$

where, $H(t)$ indicate an output of hidden layer, w_1 symbolizes a weight between the input and hidden layer, $F_i(t)$ denotes an input (i.e. feature vector), w_2 indicates weights of the hidden layers, $h(t-1)$ indicates an output of the previous hidden layer. The operator '*' denotes a convolutional operator. Finally, the output of the hidden layer is fed into the output layer.

$$Y(t) = [w_3 * H(t)] \tag{18}$$

From Eq.(18), $Y(t)$ indicates an output of deep learning, w_3 denotes a weight of the hidden and output layer, $H(t)$ represents an output of the hidden layer. In this way, the classification is performed to identify changes in the image. After classification, the error rate (E) is measured based on the squared difference between the actual and predicted errors.

$$E = |E_a - E_p|^2 \tag{19}$$

where, E_a denotes an actual error, E_p indicates a predicted error. If the architecture attains minimum error, then the process is stopped. The algorithmic process of the proposed technique is described as given below,

Algorithm 3: Tucker's Congruence Coefficient Deep Convolutional neural learning

Input: Extracted features

Output: Increase change detection rate

Begin
Step 1: Given the extracted features into **an** input layer '$x(t)$'
Step 2: Transform the features into the hidden layer to minimize the dimensions
Step 3: **For** each extracted feature '$F_i(t_i)$'
Step 4: **for each** extracted feature '$F_j(t_j)$'
Step 5: Measure Tucker's congruence correlation 'Z_{ij}'
Step 6: If (Z_{ij}=-1) **then**
Step 7: Changes are detected
Step 8: else
Step 9: Changes are not detected
Step 10: **End if**
Step 11: End for
Step 12: **End for**
Step 13: Measure error 'E'
Step 14: Repeat the process until error gets minimized

End

The step-by-step process of the proposed Tucker's Congruence Coefficient Deep Convolutional neural learning model is designed with the objective of improving change detection based on classification. This is performed using deep learning comprising of one input layer, hidden layers, and one output layer. First, the extracted features are given to the input layer. Then the input is transformed to the hidden layers for analyzing features by applying Tucker's Congruence correlation Coefficient. Based on the correlation coefficient resultant value, the changes are correctly detected with minimum error.

4. EXPERIMENTAL SETUP

The experimental evaluation of the proposed AKRGOFS-TCDCL technique and existing methods SiamCRNN [1] ADS-Net [2] are simulated by using Keras python library high-level python API. It is used to quickly build and train neural networks using Tensorflow as back-end. The input satellite images are collected from the National Remote Sensing Centre (NRSC), ISRO (http://bhuvan.nrsc.gov.in). Bhuvan is an Indian web-based service that permits the users to examine a set of map-based content organized by the Indian Space Research Organization (ISRO). ISRO has used data provided by satellites comprising the Resources at-1, Cartosat-1, and Cartosat-2 to get the best feasible images of land cover. The algorithm parameters tuning of the

AKRGOFS-TCDCL technique are considered such as learning rate of 0.03, number of hidden layers of 2, weight of 1.0, and bias of 0.1 in the ranges of a network trained.

5. PERFORMANCE RESULTS AND DISCUSSION

The performance of the proposed technique AKRGOFS-TCDCL and existing methods SiamCRNN [1] ADS-Net [2] are discussed with different metrics such as detection rate, false alarm rate, and detection time. The performances of proposed and existing methods are obtained based on the table and graphical representation.

5.1 QUALITATIVE ANALYSIS

A qualitative analysis of the proposed AKRGOFS-TCDCL technique and existing methods is illustrated with different processes.
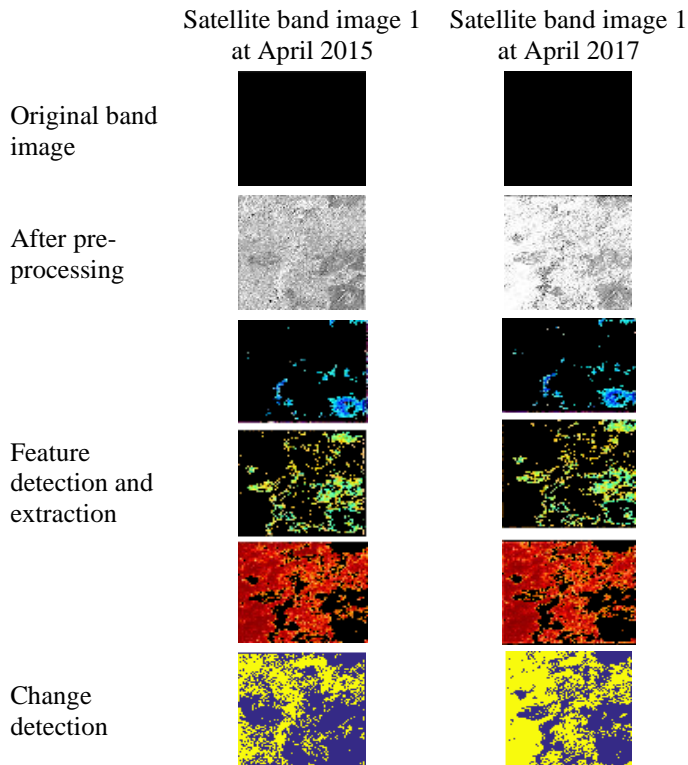

Fig.6. Qualitative results of AKRGOFS-TCDCL technique

The Fig.6 illustrates the qualitative analysis of AKRGOFS-TCDCL technique. The input pair of band images at different time interval is collected and preprocessing is carried out to improve image quality. After preprocessing, texture, intensity, and color features are extracted from band images pair. Then feature matching process is carried out using Deep Jaccard Regressive Squeezenet Convolutional network. Finally, change detection results are observed.

5.2 IMPACT OF DETECTION RATE

Detection rate is defined as the rate of changes observed in given input images correctly identified by algorithm to total number of images taken as input. The Detection rate is calculated using a given formula,

$$DR=100*((\text{changes in images are correctly detected})/n) \quad (20)$$

where DR denotes a detection rate, n represents the number of images. The detection rate is measured in terms of percentage (%).

5.2.1 Sample Calculation Using Detection Rate:

- **Proposed AKRGOFS-TCDCL technique:** Consider 10 input images, changes in images are correctly detected as '8'. The detection rate is estimated as,

$$DR=((8)/10)*100=80\%$$

- **Existing Siam CRNN:** Consider 300 input images, changes in images are correctly detected as '6'. The detection rate is estimated as,

$$DR=((6)/10)*100=60\%$$

- **Existing ADS-Net:** Consider 300 input images, changes in images are correctly detected as '7'. The detection rate is estimated as,

$$DR=(7/10)*100=70\%$$

Table.1. Detection Rate

Band Image Pairs (Numbers)	Detection rate (%)		
	AKRGOFS-TCDCL	Siam CRNN	ADS-Net
10	80	60	70
20	85	75	80
30	87	80	83
40	90	83	85
50	92	82	86
60	92	85	88
70	91	84	87
80	93	86	88
90	93	87	89
100	92	87	88

The Table.1 provides performance results of detection rate along with the number of band images pairs taken in the ranges of 10 to 100 from the dataset. For each method, ten different results are observed. The obtained results indicate that the change detection rate of the AKRGOFS-TCDCL technique is higher than existing methods SiamCRNN [1] ADS-Net [2]. Let us consider 10 band images pairs in the first iteration. By applying the AKRGOFS-TCDCL technique, changes are correctly detected in 8 images pairs and the detection rate is 80%. Whereas, the changes are correctly detected in 6 and 7 band images using [1] [2] and the detection rate is 60% and 70% respectively. Similarly, various results are obtained for different pairs of band images. For each method, ten different outcomes are observed. The observed results indicate that AKRGOFS-TCDCL technique outperforms well in terms of achieving higher detection rate. The performance of the proposed technique is compared to existing methods. The comparison results show that the change detection rate of proposed technique is comparatively increased by 11% to SiamCRNN [1] and 6% to ADS-Net [2] respectively.

The Table.1 illustrates the performance analysis of detection rate along with the number of band images pairs in the ranges from 10 to 100. As shown in Table.1, the numbers of band images are taken in the horizontal axis and the detection rate is observed in the vertical direction. As shown in the graphical chart, three various colors of lines such as green, blue and red indicate the detection rate of three techniques namely AKRGOFS-TCDCL technique is higher than existing methods SiamCRNN [1] ADS-Net [2] respectively. Compared to the other two existing methods, the proposed AKRGOFS-TCDCL technique has the ability of increasing the detection rate. The significant reason for this improvement is the application of Tucker's congruence coefficient deep convolutional neural learning classifier. Tucker's congruence correlation coefficient analyzes the extracted features from the two band images. Based on feature matching, the changes in the given satellite images are correctly detected with higher accuracy.

5.3 IMPACT OF FALSE ALARM RATE

False alarm rate is measured as the changes in the given input images correctly detected to the total number of images considered as input. Therefore, the false alarm rate is calculated using a given formula,

$$FAR=100*[(\text{changes in images are incorrectly detected })/n] \quad (21)$$

From Eq.(21), FAR indicates a false alarm rate, 'n' represents the number of images. The False alarm rate is measured in the unit of percentage (%).

5.3.1 Sample Calculation Using False Alarm Rate

• **Proposed AKRGOFS-TCDCL technique:** Consider 10 input images, changes in images are incorrectly detected as '2'. The false alarm rate is measured as,

$$FAR=(2/10)*100=20\%$$

• **Existing Siam CRNN:** Consider 300 input images, changes in images are incorrectly detected as '4'. The false alarm rate is measured as,

$$FAR=((4\ )/10)*100=40\%$$

• **Existing ADS-Net:** Consider 300 input images, changes in images are incorrectly detected as '3'. The false alarm rate is measured as,

$$FAR=(3/10)*100=30\%$$

Table.2. False alarm rate

Band image pairs (numbers)	False alarm rate (%)		
	AKRGOFS-TCDCL	SiamCRNN	ADS-Net
10	20	40	30
20	15	25	20
30	13	20	17
40	10	18	15
50	8	18	14
60	8	15	12
70	9	16	13
80	8	14	13
90	7	13	11
100	8	13	12

Experimental results of the false-alarm rate of three different methods namely AKRGOFS-TCDCL technique, SiamCRNN [1] ADS-Net [2] are given in above table. In order to conduct the experiment, we choose 100 band image pairs for each method and ten different results are observed. The observed results reveal that the false-alarm rate of the change detection using the namely AKRGOFS-TCDCL technique is lesser than the other methods. This is quantitatively confirmed by considering the 10 images. From the input, 2 images are incorrectly categorized and the false-alarm rate is 20% using the AKRGOFS-TCDCL technique. Similarly, 3 and 4 images are incorrectly classified and the false-alarm rate is 30% and 40% using SiamCRNN [1] ADS-Net [2]. The obtained results of the proposed AKRGOFS-TCDCL technique are compared to conventional methods. The average of ten comparative values demonstrates that the false-alarm rate is considerably decreased by 44% and 33% when compared to existing methods.

The Table.2 demonstrates the performance analysis of false-alarm rate with respect to the number of band image pairs. As revealed in the above graphical chart, the proposed AKRGOFS-TCDCL technique outperforms well in terms of achieving lesser false-alarm rate than the other two classification methods. The reason for minimum false-alarm rate is the application of Tucker's congruence correlation. The correlation function matches the features extracted from the pair of band images. Then with the feature matching process of the proposed AKRGOFS-TCDCL technique via correlation function minimizes the incorrect classification hence the false alarm rate is decreased.

5.4 IMPACT OF DETECTION TIME

Detection time is calculated as the amount of time taken by an algorithm to detect various changes in the homogeneous satellite images. The overall detection time is measured as follows,

$$DT=[n]*\text{time}(DC_s) \quad (22)$$

From Eq.(22), DT denotes a detection time, n represents the number of images, DC_s denotes a change detection using one pair of images. The detection time is measured in milliseconds (ms).

5.4.1 Sample Calculation Using Detection Time

• **Proposed AKRGOFS-TCDCL technique:** Consider 10 input images, the amount of time required to detect various changes is 0.09. The detection time is computed as,

$$DT= 10*1.8=18\text{ms}$$

• **Existing Siam CRNN:** Consider 300 input images, the amount of time required to detect various changes is 0.09. The detection time is computed as,

$$DT= 10*2.2=22\text{ms}$$

• **Existing ADS-Net:** Consider 300 input images, the amount of time required to detect various changes is 0.09. The detection time is computed as,

$$DT= 10*2=20\text{ms}$$

Table.3. Detection time

Band image pairs (numbers)	Detection time (ms)		
	AKRGOFS-TCDCL	SiamCRNN	ADS-Net
10	18	22	20
20	24	30	26
30	27	36	33
40	34	40	38
50	41	48	45
60	45	53	48
70	49	56	53
80	52	60	56
90	56	62	59
100	60	65	62

The Table.3 depicts performance results of change detection time against the number of band image pairs taken from the dataset. The tabulated results reveal that the time taken for change detection time is considerably decreased using AKRGOFS-TCDCL technique than the other two conventional methods. Let us consider 10 Band image pairs for experimentation, the time consumed by AKRGOFS-TCDCL technique to detect the changes is 18ms, whereas '22ms and 20ms of time consumed by existing techniques SiamCRNN [1] ADS-Net [2]. Therefore, the overall results of the proposed AKRGOFS-TCDCL technique are compared to other classification techniques. The average of ten comparison results demonstrates that the change detection time is considerably reduced by 15% and 8% than the state-of-the-art methods.

The performance analysis of change detection time with number of band image pairs is shown in Table.3. As exposed in the graphical chart, change detection time is progressively increased for all three methods while increasing the number of band images since the input counts of images get increased for each run. Alternatively, the change detection time of each method gets increased while increasing the number of images. From the detected results, it is obvious that the change detection time is reduced using the AKRGOFS-TCDCL technique. The time minimization is achieved by applying preprocessing steps as well as feature selection, extraction. In the preprocessing steps, various corrections are obtained to increase the image quality. Followed by, feature selection and extraction process minimize time consumption. Finally, the classification is performed with the extracted features for detecting the changes in the given satellite images with minimum time.

5.5 IMPACT OF PEAK SIGNAL TO NOISE RATIO

Peak Signal to Noise Ratio (PSNR) is measured based on the mean square error. It is determined as the difference between pre-processed image and the original image. PSNR is computed in terms of decibel (dB). The PSNR is mathematically expressed as given below:

$$MSE=(Original\ image\ size\text{-Preprocessed image size})^2 \quad (23)$$
$$PSNR=10\log_{10}(R^2/MSE) \quad (24)$$

From Eq.(24), peak signal to noise ratio 'PSNR' is computed with the use of 'MSE' mean square rate. In Eq.(23), mean square rate is estimated. Here, 'R' represented as maximum image pixel point and the value of 'R' is 255.

5.5.1 Sample Calculation Using Peak Signal to Noise Ratio

- **Proposed AKRGOFS-TCDCL technique**: original image size is 22.2KB and the pre-processed image size is $22KB$. Then, the mean square error, and peak signal to noise ratio is measured as,

$$MSE=(22.2\text{KB-22 KB})^2=0.04$$
$$PSNR=10\log_{10}(255^2/0.04)=62.11db$$

- **Existing Siam CRNN**: original image size is 22.2KB and the pre-processed image size is $21.9\ KB$. With the aid of above values, the mean square error, and peak signal to noise ratio is determined as,

$$MSE=(22.2\text{KB-21.9KB})^2=0.09$$
$$PSNR=10\log_{10}(255^2/0.09)=58.58\ db$$

- **Existing ADS-Net**: original image size is 22.2KB and the pre-processed image size is $21.6KB$. With the aid of above values, the mean square error, and peak signal to noise ratio is determined as,

$$MSE=(22.2\text{KB-21.6KB})^2=0.36$$
$$PSNR=10\log_{10}(255^2/0.36)=52.56db$$

Table.4. Peak Signal to Noise Ratio

Image size (KB)	Peak Signal to Noise Ratio (dB)		
	AKRGOFS-TCDCL	SiamCRNN	ADS-Net
22.2	62.11	58.58	52.56
22.48	63.02	56.53	54.5
23.5	56.08	54.15	51.22
23.7	61.28	58.58	54.15
24.4	64.6	62.11	58.58
24.9	56.08	52.56	51.22
25.5	62.11	58.58	56.08
26.2	68.13	62.11	58.58
27.6	63.52	59.18	55.26
28.9	62.11	56.08	52.56

The Table.4 illustrates the experimental evaluation of peak signal to noise based on the different sizes of the input in terms of kilo bytes (KB). Totally ten iterations are described as shown in Table.4. The results of three methods namely AKRGOFS-TCDCL technique, SiamCRNN [1], and ADS-Net [2] are shown in table. Among the three methods, the findings of peak signal to noise ratio is found to be higher using AKRGOFS-TCDCL technique. The improvement of the AKRGOFS-TCDCL technique is achieved by applying the adaptive kuan filtering. The filtering result concludes that the unwanted noisy pixels. The final obtained results showed that the contrast enhanced image used for change detection. The AKRGOFS-TCDCL technique also minimizes the mean square error. The comparison results displays that the peak signal to noise ratio is found to be significantly improved by 7% and 10% when compared to SiamCRNN [1], and ADS-Net [2].

The Table.4 reveals the performance analysis of the peak signal to noise ratio obtained by using the proposed AKRGOFS-TCDCL technique, and the two existing methods namely SiamCRNN [1], and ADS-Net [2] respectively. For a better presentation, ten various samples (i.e., band image) were taken from the database. The various performance results of peak signal to noise ratio are represented by the different colors of lines namely blue, red, and green respectively. As illustrated in Table.4, that the peak signal to noise ratio achieved using our proposed technique is better than the peak signal to noise ratio of using the state-of-the-arts techniques. The reason for this improvement in peak signal to noise ratio is due to the ability of improving the image contrast by using the adaptive kuan filtering.

6. CONCLUSION

This paper presents a novel change detection technique called AKRGOFS-TCDCL is for satellite images. Our objective is to introduce an algorithm based on different processes for improving change detection with minimum time consumption. First, image preprocessing is carried out for performing different corrections such as Atmospheric corrections, radiometric correction, Topographic correction, and image contrast enhancement using e Adaptive Kuan filtering technique. The Dichotomous probit Regressive gene optimization is then applied to discover optimal feature and extract various features such as texture, color, and intensity for reducing time involved in detecting changes. Finally, Tucker's congruence coefficient deep convolutional neural learning classifier is applied for identifying different changes in the specified satellite images with the help of feature matching. Based on the classified results, accurate change detection is performed with minimum time. The comprehensive experimental evaluation is carried out with satellite images. The quantitative and qualitative results verified the advantages of the AKRGOFS-TCDCL technique in terms of higher detection rate and lesser time as well as false alarm rate when compared to other related methods. The proposed techniques are employed to perform different corrections but, the image quality is not enhanced. In future work, various filtering techniques are applied for improving the image quality.

REFERENCES

[1] Hongruixuan Chen, Chen Wu, Bo Du, Liangpei Zhang and Le Wang, "Change Detection in Multisource VHR Images via Deep Siamese Convolutional Multiple-Layers Recurrent Neural Network", *IEEE Transactions on Geoscience and Remote Sensing*, Vol. 58, No. 4, pp. 2848-2864, 2020.

[2] Decheng Wang, Xiangning Chen, Mingyong Jiang, Shuhan Du, Bijie Xu and Junda Wang, "ADS-Net: An Attention-Based Deeply Supervised Network for Remote Sensing Image Change Detection", *International Journal of Applied Earth Observation and Geoinformation*, Vol. 101, pp. 1-7, 2021.

[3] Suicheng Li, Pengcheng Han, Shuhui Bu, Pinmo Tong, Qing Li, Ke Li and Gang Wan, "Change Detection in Images using Shape-Aware Siamese Convolutional Network", *Engineering Applications of Artificial Intelligence*, Vol. 94, pp. 1-11, 2020.

[4] Walma Gharbi, Lotfi Chaari and Amel Benazza-Benyahia, "Unsupervised Bayesian Change Detection for Remotely Sensed Images", *Signal, Image and Video Processing*, Vol. 15, pp. 205-213, 2021.

[5] Rui Zhao, Guo-Hua Peng, Wei-Dong Yan, Lu-Lu Pan and Li-Ya Wang, "Change Detection in SAR Images based on Superpixel Segmentation and Image Regression", *Earth Science Informatics*, Vol. 14, pp. 69-79, 2021.

[6] Huihui Dong, Wenping Ma, Yue Wu, Jun Zhang and Licheng Jiao, "Self-Supervised Representation Learning for Remote Sensing Image Change Detection Based on Temporal Prediction", *Remote Sensing*, Vol. 12, pp. 1-38, 2020.

[7] Tengfei Bao, Chenqin Fu, Tao Fang and Hong Huo, "PPCNET: A Combined Patch-Level and Pixel-Level End-to-End Deep Network for High-Resolution Remote Sensing Image Change Detection", *IEEE Geoscience and Remote Sensing Letters*, Vol. 17, No. 10, pp. 1797-1801, 2020.

[8] Neelam Ruhil, Mohan Singh, Debjani Mitra, Akansha Singh and Krishna Kant Singh, "Detection of Changes from Satellite Images using Fused Difference Images and Hybrid Kohonen Fuzzy C-Means Sigma", *Procedia Computer Science*, Vol. 167, pp. 431-439, 2020.

[9] Dawei Li, Siyuan Yan, Mingbo Zhao and Tommy W.S. Chow, "Spatiotemporal Tree Filtering for Enhancing Image Change Detection", *IEEE Transactions on Image Processing*, Vol. 29, pp. 8805-8820, 2020.

[10] Chinmayee Pati, Ashok K. Panda, Ajaya Kumar Tripathy, Sateesh K. Pradhan and Srikanta Patnaik, "A Novel Hybrid Machine Learning Approach for Change Detection in Remote Sensing Images", *Engineering Science and Technology, an International Journal*, Vol. 23, No. 5, pp. 973-981, 2020.

[11] S. Kalaiselvi and V. Gomathi, "α-Cut Induced Fuzzy Deep Neural Network for Change Detection of SAR Images", *Applied Soft Computing*, Vol. 95, pp. 1-26, 2020.

[12] Junfu Liu, Keming Chen, Guangluan Xu, Xian Sun, Menglong Yan, Wenhui Diao and Hongzhe Han, "Convolutional Neural Network-Based Transfer Learning for Optical Aerial Images Change Detection", *IEEE Geoscience and Remote Sensing Letters*, Vol. 17, No. 1, pp. 127-131, 2020.

[13] Ming Hao, Mengchao Zhou, Jian Jin and Wenzhong Shi, "An Advanced Superpixel-Based Markov Random Field Model for Unsupervised Change Detection", *IEEE Geoscience and Remote Sensing Letters*, Vol. 17, No. 8, pp. 1401-1405, 2020.

[14] Yun Lin, Shutao Li, Leyuan Fang and Pedram Ghamisi, "Multispectral Change Detection with Bilinear Convolutional Neural Networks", *IEEE Geoscience and Remote Sensing Letters*, Vol. 17, No. 10, pp. 1757-1761, 2020.

[15] Shiming Xiang and Bo Tang, "Kernel-Based Edge-Preserving Methods for Abrupt Change Detection", *IEEE Signal Processing Letters*, Vol. 27, pp. 86-90, 2019.

[16] Wahyu Wiratama, Jongseok Lee and Donggyu Sim, "Change Detection on Multi-Spectral Images Based on Feature-level U-Net", *IEEE Access*, Vol. 8, pp. 12279-12289, 2020.

[17] Dawei Li, Siyuan Yan, Xin Cai, Yan Cao and Sifan Wang, "An Integrated Image Filter for Enhancing Change Detection Results", *IEEE Access*, Vol. 7, pp. 91034-91051, 2019.

[18] Jia Liu, Maoguo Gong, A.K. Qin and Kay Chen Tan, "Bipartite Differential Neural Network for Unsupervised Image Change Detection", *IEEE Transactions on Neural Networks and Learning Systems*, Vol. 31, No. 3, pp. 876-890, 2020.

[19] Zhi Lia, Zhenhong Jiaa, Luyang Liua, Jie Yanga and Nikola Kasabov, "A Method to Improve the Accuracy of SAR Image Change Detection by using an Image Enhancement Method", *ISPRS Journal of Photogrammetry and Remote Sensing*, Vol. 163, No. 4, pp. 137-151, 2021.

[20] Yi Zhang, Lei Fu, Ying Li and Yanning Zhang, "HDFNet: Hierarchical Dynamic Fusion Network for Change Detection in Optical Aerial Images", *Remote Sensing*, Vol. 13, pp. 1-22, 2021.